

Inertial consistent subgrid model for large-eddy simulation based on the lattice Boltzmann method

Yu-Hong Dong,^{1,2} Pierre Sagaut,^{2,a)} and Simon Marie^{2,3}

¹Shanghai Institute of Applied Mathematics and Mechanics, Shanghai University, Shanghai 200072, China

²Institut Jean Le Rond d'Alembert, Université Pierre et Marie Curie-Paris 6, F-75252 Paris Cedex 5, France

³Technocentre Renault, TCR AVA 163, 01 Avenue du Golf, F-78288 Guyancourt, France

(Received 19 July 2007; accepted 10 January 2008; published online 10 March 2008)

The recently introduced inertial-range (IR) consistent Smagorinsky model and the classical Smagorinsky model are applied to the large-eddy simulation (LES) of decaying homogeneous isotropic turbulence based on the lattice Boltzmann method (LBM), which is implemented using the 19-velocity D3Q19 lattice model. The objectives of this study are to examine the effectiveness of the LES-LBM technique for study of turbulence and to extend and validate the efficiency of the inertial-range consistent Smagorinsky model for lattice Boltzmann fluid dynamics. The LES-LBM results are compared with the direct numerical simulation data as well as experimental data. The time evolution of the kinetic energy and the decay exponents of the dissipation rate, the velocity derivative skewness, and instantaneous energy spectra are analyzed. The dependency of behavior of the model coefficients on the ratio of grid width Δ and the Kolmogorov scale η is examined numerically. The results demonstrate that the LES-LBM in conjunction with the IR consistent Smagorinsky model can be used to simulate turbulence more satisfactorily than the standard Smagorinsky model. © 2008 American Institute of Physics. [DOI: 10.1063/1.2842379]

I. INTRODUCTION

The lattice Boltzmann method (LBM) appears to be a very attractive model to compute flows in the low subsonic regime, and it has been applied successfully in many areas of flow physics, such as various laminar flows, flows with interface or heat transfer, multicomponent flows, two-phase flows, viscoelastic fluids, and other complex flows.^{1,2} The method, which is based on the Boltzmann transport equation for the time rate of change of the particle distribution function, is regarded as one of the simplest mesoscopic approaches for modeling macroscopic dynamical phenomena.^{3–6} Furthermore, Navier–Stokes (NS) equations can be derived from the lattice Boltzmann equation (LBE) when the Chapman–Enskog multiscale and small parameter expansion is used.^{4,6} The one greatest advantage of this method is that it is very well suited for computation on massively parallel computers since the computational stencil is compact and time advancement is explicit.² Therefore, the LBM appears as a powerful alternative to the standard Navier–Stokes-based approaches to model the behavior of complex physical systems.

Despite the exponentially growing literature devoted to the LBM, its progress in studying turbulent flow is not fully satisfactory compared with its achievements in other aspects at present. In particular, it appears that large-eddy simulation (LES) has not been adequately developed in the LBM framework. One important reason is the lack of turbulence subgrid-scale (SGS) models suited for this approach. Indeed, there have been some preliminary studies^{7–11} devoted to the

development of LES-LBM in recent years, with hope that it can solve efficiently aerodynamic, hydrodynamic, and aeroacoustic problems. Therefore, it is reasonable to believe that the theory and numerical experiments that aim at the development of efficient LES-LBM based on various SGS models will be of more interest and would greatly enrich strategies for the study of turbulent flows.

Homogenous isotropic turbulence (HIT) has long served as a core of turbulence research as well as an important benchmark test case for turbulence theories, experiments, models, and simulations.^{12–20} But, unlike those traditional finite-difference or spectral methods, there are only a few simulations of HIT performed with the LBM.^{21–24} Recently, Djenidi²¹ carried out the first DNS-LBM of grid-generated turbulence. The study of Burattini *et al.*²² emphasized the power law of the energy decay rate of decaying isotropic turbulence at low Reynolds number with direct numerical simulation (DNS). Girimaji and his collaborators²³ performed a LES study with the classical Smagorinsky eddy-viscosity model to investigate decaying isotropic turbulence with and without rotation and yielded encouraging results. They also studied homogeneous turbulence subjected to periodic shear as well as compressible isotropic turbulence with temperature fluctuations by DNS-LBM.^{24,25} More recently, Girimaji²⁶ further developed a kinetic Boltzmann equation for describing filtered fluid turbulence applicable for continuum and noncontinuum effects. Nevertheless, it appears that the issues of investigating behavior of different SGS models and the effect of model coefficients on the simulations have received little attention.

The behavior of subgrid models in well resolved and/or low-Reynolds turbulent flows is known to be nontrivial,

^{a)}Author to whom correspondence should be addressed. Electronic mail: Pierre.sagaut@upmc.fr.

which yielded the development of dynamic subgrid models^{27,28} and more recently of inertial range (IR) consistent subgrid models.^{29,30} In this paper, we propose to extend the mapping technique developed by Meyers and Sagaut²⁹ to recover an IR consistent Smagorinsky model to the LBM framework. The decaying homogeneous isotropic turbulence (DHIT) is selected as a test case. The first objective is to investigate the sensitivity of turbulence evolution on the various Smagorinsky SGS models, the model coefficients, and the grid resolution. The second objective is to validate further the efficiency and the accuracy of LES-LBM. In addition, different from most of the DHIT cases available in the literature in which an isotropic Gaussian field is utilized as an initial condition, it is proposed here to use a numerically consistent initial velocity field based on the actual initial energy spectra deduced from the measurements of the experiment by Kang *et al.*³¹

This paper is organized as follows: The mathematical formulation including the fundamentals of the lattice Boltzmann method, LES extension of the LBM, and the variants of the Smagorinsky model are described in Sec. II. The details of the numerical procedure and initial conditions are given in Sec. III. In Sec. IV, the instantaneous energy spectrum is analyzed first. Then some statistical quantities, including the decay exponents of the kinetic energy and the dissipation rate, and validations based on the comparison with existing results of measurements, are given. The time evolution of velocity derivative skewness and flatness is discussed. The performance of the variants of the Smagorinsky model with different model coefficients and grid resolutions

is reported. Finally, concluding remarks are summarized in Sec. V.

II. MATHEMATICAL FORMULATIONS

A. Lattice Boltzmann method

We simulate the decaying homogeneous isotropic turbulence using the lattice Boltzmann method with the multi-block and multiprocessors parallel technique. Here, the lattice Boltzmann equation for the discrete velocity distribution is solved using the single relaxation time approximation following Bhatnagar, Gross, and Krook (BGK)³² as

$$f_{\alpha}(\mathbf{x} + \mathbf{e}_{\alpha}\delta t, t + \delta t) - f_{\alpha}(\mathbf{x}, t) = -\frac{1}{\tau}[f_{\alpha}(\mathbf{x}, t) - f_{\alpha}^{(e)}(\mathbf{x}, t)]. \quad (1)$$

The evolution process of the LBM algorithm has the following two steps: Collision (relaxation toward equilibrium) and streaming (shifting data between lattice sites). Here, $f_{\alpha}(\mathbf{x}, t)$ is the distribution function at a node \mathbf{x} and time t with particle velocity vector \mathbf{e}_{α} , and τ is relaxation time due to particle collisions that control the rate of approach to equilibrium. This method solves the lattice Boltzmann equation (LBGK)^{4,6} on each lattice by construction of a simplified kinetic model that conserves the essential physical properties of macroscopic average quantities, such as mass and momentum.

In the present studies, a cubic lattice model D3Q19 is used to simulate the homogeneous isotropic turbulence. This model is composed of one zero and 18 nonzero discrete particle velocities at each computational lattice.³³ The corresponding discrete velocities \mathbf{e}_{α} are given by

$$\mathbf{e}_{\alpha} = \begin{cases} (0,0,0) & \alpha = 0 \\ (\pm 1, 0, 0)c, & (0, \pm 1, 0)c, & (0, 0, \pm 1)c & \alpha = 1 \sim 6 \\ (\pm 1, \pm 1, 0)c, & (\pm 1, 0, \pm 1)c, & (0, \pm 1, \pm 1)c & \alpha = 7 \sim 18 \end{cases} \quad (2)$$

$f_{\alpha}^{(e)}(\mathbf{x}, t)$ in Eq. (1) is the local equilibrium distribution function at each node,⁵

$$f_{\alpha}^{(e)}(\mathbf{x}, t) = \rho\omega_{\alpha} \left\{ 1 + 3 \left[\frac{\mathbf{e}_{\alpha} \cdot \mathbf{u}}{c^2} + \frac{3(\mathbf{e}_{\alpha} \cdot \mathbf{u})^2}{2c^4} - \frac{u^2}{2c^2} \right] \right\}, \quad (3)$$

where ω_{α} are corresponding weights,

$$\omega_{\alpha} = \begin{cases} 1/3 & \alpha = 0 \\ 1/18 & \alpha = 1 \sim 6 \\ 1/36 & \alpha = 7 \sim 18 \end{cases} \quad (4)$$

The mass density ρ and macroscopic local velocity \mathbf{u} are defined in terms of the particle distribution function by

$$\rho(\mathbf{x}, t) = \sum_{\alpha} f_{\alpha}(\mathbf{x}, t), \quad (5)$$

$$\rho(\mathbf{x}, t)\mathbf{u}(\mathbf{x}, t) = \sum_{\alpha} \mathbf{e}_{\alpha} f_{\alpha}(\mathbf{x}, t). \quad (6)$$

Pressure can be obtained from the equation of state as $p = \rho c_s^2$. The kinematic viscosity ν depends on the lattice relaxation time τ as follows:

$$\nu = \left(\tau - \frac{1}{2} \right) c_s^2 \delta t, \quad (7)$$

where the sound speed is $c_s = c/\sqrt{3}$ in the lattice Boltzmann model,^{4,6} and c is the ratio of the lattice space step δx and the time step δt , respectively, $c = \delta x/\delta t$. The property of the viscosity requires that the relaxation time $\tau > 1/2$ in the LBE computations.

B. The lattice Boltzmann scheme with large-eddy simulation

In LES-LBM, different from the DNS-LBM, the practical relaxation time should be adjusted locally, according to the local and temporal resolved mean strain tensor. This is equivalent to Prandtl's mixing length theory in which the mean free path of the particle will be affected by the local strain intensity.¹⁰ In other words, an additive space and time variable relaxation time scale τ_τ (related to the turbulent eddy-viscosity ν_τ) is introduced into the effective relaxation time τ_w . The filtered lattice Boltzmann equation for LES is written as

$$\bar{f}_\alpha(\mathbf{x} + \mathbf{e}_\alpha \delta t, t + \delta t) - \bar{f}_\alpha(\mathbf{x}, t) = -\frac{1}{\tau_w} [\bar{f}_\alpha(\mathbf{x}, t) - \bar{f}_\alpha^{(e)}(\mathbf{x}, t)], \quad (8)$$

where τ_w should be a function of the total viscosity ν_w , which is equal to the sum of the subgrid eddy viscosity ν_τ and the molecular viscosity ν_0 ,

$$\tau_w = \frac{1}{2} + \frac{\nu_w}{c_s^2 \delta t} = \frac{1}{2} + \frac{1}{c_s^2 \delta t} (\nu_\tau + \nu_0). \quad (9)$$

It is well known that the overall expression of the classical Smagorinsky model is based on the eddy viscosity assumption,³⁵

$$\tau_{ij} - \frac{\delta_{ij}}{3} \tau_{ij} = -2\nu_\tau \bar{S}_{ij}, \quad (10)$$

where $\tau_{ij} = \overline{u_i u_j - \bar{u}_i \bar{u}_j}$ is the subgrid Reynolds stress, which represents the effect of the subgrid scales on the resolved scales. Smagorinsky³⁵ suggested the expression of ν_τ by supposing that the eddy viscosity is proportional to the characteristic length and the velocity of the small scales. Thus, ν_τ is calculated from the filtered strain rate,

$$\nu_\tau = (C\Delta_L)^2 |\bar{S}|. \quad (11)$$

The strain rate tensor is $\bar{S}_{ij} = (\partial \bar{u}_i / \partial x_j + \partial \bar{u}_j / \partial x_i) / 2$, $|\bar{S}| = [2\bar{S}_{ij}\bar{S}_{ij}]^{1/2}$. Here, Δ_L denotes the filter width equal to the length scale of a uniform mesh, $\Delta_L = \delta x = \delta y = \delta z$. C is the Smagorinsky constant. To implement the SGS eddy-viscosity model, substituting Eq. (11) into Eq. (9), one has

$$\tau_w = \frac{1}{2} + \frac{1}{c_s^2 \delta t} [\nu_0 + C^2 \Delta_L^2 |\bar{S}|]. \quad (12)$$

One must first evaluate the local intensity of the strain tensor $|\bar{S}|$ to compute the relaxation time τ_w . There are at least two methods for calculation of $|\bar{S}|$.¹⁰ The first one is to compute the finite-difference approximation of the velocity gradients, the velocity field being obtained at each lattice time step thanks to Eq. (6). Another way is to evaluate it directly from the nonequilibrium properties of the filtered particle distribution function, that is to say, the strain rate tensor \bar{S}_{ij} is related to the momentum flux tensors, i.e., the nonequilibrium stress tensor \bar{Q}_{ij} , as follows:¹⁰

$$\bar{S}_{ij} = -\frac{1}{2\rho_0 c_s^2 \tau_w} \bar{Q}_{ij}, \quad (13)$$

$$\bar{Q}_{ij} = \sum_\alpha e_{\alpha i} e_{\alpha j} [\bar{f}_\alpha - \bar{f}_\alpha^{(e)}], \quad (14)$$

where $e_{\alpha i}$ is the discrete velocity in the αi direction. Substituting Eq. (12) in the following equation:

$$|\bar{Q}| = 2\rho_0 c_s^2 \tau_w |\bar{S}|,$$

where $\bar{Q} = (2\bar{Q}_{ij}\bar{Q}_{ij})^{1/2}$, and we obtain

$$|\bar{S}|^2 + \frac{c_s^2 \tau_0 \delta t}{C^2 \Delta_L^2} |\bar{S}| - \frac{\delta t}{2C^2 \Delta_L^2} |\bar{Q}| = 0. \quad (15)$$

Following this second method, we can obtain $|\bar{S}|$ by Eq. (15) when the magnitude of the current nonequilibrium stress tensor $|\bar{Q}|$ is calculated from Eq. (14), and substituting it into Eq. (12), we have

$$\tau_w = \frac{1}{2} + \frac{1}{c_s^2 \delta t} \times \left\{ \nu_0 + \frac{c_s^2}{2} \left[\sqrt{\tau_0^2 \delta t^2 + 2c_s^{-4} \delta t C^2 \Delta_L^2 |\bar{Q}|} - \tau_0 \delta t \right] \right\}. \quad (16)$$

In the LES-LBM with a uniform mesh, $c = \delta x / \delta t = 1$, leading to $c_s^2 = 1/3$. The total effective relaxation time τ_w used in filtered LBE (8) is calculated from Eq. (16) once the Smagorinsky constant C , the lattice length unit Δ_L , and the kinematic viscosity ν_0 are given.

C. An IR consistent Smagorinsky model

An important aim in the present study is to extend the inertial-range (IR) consistent variant of the Smagorinsky model for the lattice Boltzmann scheme and to assess this new improved model. To this end, it is chosen to compare the results obtained using this model with those of the traditional Smagorinsky model in which subgrid viscosity is obtained employing Lilly's classical theoretical analysis.³⁶ By assuming that the grid spacing lies within the inertial subrange, he calculated the rate at which the Smagorinsky model transfers energy to the subgrid scales, and obtained a theoretical prediction of constant C equating the rate of energy transfer with the dissipation rate ε . He obtained the value $C=0.18$ in the finite-difference approximation. The IR consistent model concept was introduced by Meyers and Sagaut,²⁹ with application to the standard and two variational multiscale Smagorinsky models. Here we will provide a brief description specialized for the case of a LES-LBM. The study showed that the inertial-range behavior of the model coefficient C strongly depends on two important parameters, namely the local ratio of the LES-filter width Δ and the Kolmogorov scale η , and the ratio of the integral length scale L and Δ . The dependence on these two parameters may be used in a different way, and the use of η/Δ -dependent model coefficients was expressed as²⁹

$$C = C_\infty \Phi^{-3/4} \sqrt{1 - (\gamma \eta / C_\infty)^{-4/3} \Phi / \gamma}, \quad (17)$$

where γ is a parameter that depends only on the shape of the filter kernel G (see Ref. 29 for details),

$$\gamma = \left\{ \frac{4}{3} \int_0^\infty k^{1/3} [G(k)]^2 dk \right\} / (\pi / \Delta). \quad (18)$$

The auxiliary function Φ is defined as

$$\Phi \left(\frac{L}{\Delta}, \text{Re}_L \right) = \frac{\int_0^\infty x^{1/3} [G(x/L)]^2 f_l(x) f_\eta(x \text{Re}_L^{-3/4}) dx}{\int_0^\infty x^{1/3} [G(x/L)]^2 dx}, \quad (19)$$

where Re_L is the Reynolds number based on the integral length scale $L = E^{2/3} / \varepsilon$. $G(k)$ is a transfer function associated with the filter kernel with the auxiliary variable x corresponding to kL . More details on the definition of spectrum shape functions $f_L(x)$ and $f_\eta(x)$ can be found in Pope.³⁷ To obey the numerical viability principle, the previous expression cannot be directly used in practical LES. To recover IR consistent subgrid models, the following classical Smagorinsky subgrid viscosity remapping model was introduced:²⁹

$$\nu_\tau^* = \sqrt{(C_\infty \Delta / \gamma)^4 \langle 2\bar{S}_{ij}\bar{S}_{ij} \rangle + \nu_0^2} - \nu_0. \quad (20)$$

Here, $C_\infty = 0.18$ is the theoretical constant of the Smagorinsky model related to a hypothesis of infinite Reynolds number. The parameter γ is set equal to 1 below for the sake of convenience without any law of generality. Thus, the total viscosity ν_w^* is

$$\nu_w^* = \sqrt{(C_\infty \Delta / \gamma)^4 \langle 2\bar{S}_{ij}\bar{S}_{ij} \rangle + \nu_0^2}. \quad (21)$$

One can obtain ν_w^* from Eq. (21) as far as the strain rate tensor $|\bar{S}|$ is known. Then the effective relaxation time τ_w^* used in Eq. (8) is obtained as

$$\tau_w^* = \frac{1}{2} + \frac{3}{c^2 \delta t} \nu_w^* = \frac{1}{2} + \frac{3}{c^2 \delta t} (\nu_0 + \nu_\tau^*). \quad (22)$$

According to Eqs. (13) and (22), we can obtain the following IR consistent relationship between $|\bar{S}|$ and $|\bar{Q}|$:

$$(C_\infty \Delta)^4 |S|^4 + \left(\nu_0^2 - \frac{c_s^4 \delta t^2}{4} \right) |S|^2 + \frac{c_s^2 \delta t^2 |Q|}{2} |S| - \frac{\delta t^2 |Q|^2}{4} = 0. \quad (23)$$

Here, we prefer the first way referred to in Sec. II B, i.e., $|\bar{S}|$ is evaluated from velocity field by the finite-difference method (FDM) for the sake of simplicity and avoid solving a quartic nonlinear equation for $|\bar{S}|$.

III. SELECTED CASES AND INITIAL CONDITIONS

Isotropic, isothermal decaying turbulence in a cubic box domain $[0, 2\pi]^3$ is considered. We carry out the simulations with double precision and with various resolutions N^3 , where N denotes the number of grid points in a space direction. Periodic boundary conditions are employed in the three directions.

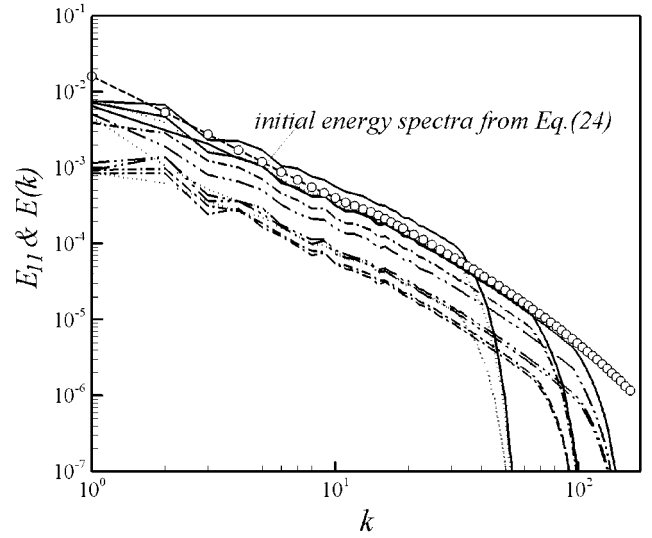


FIG. 1. Initial energy spectra from the experiment of Kang *et al.* (Ref. 31) in decaying isotropic turbulence. The one-dimensional spectra $E_{ii}(k)$ in 64^3 (dotted lines), 128^3 (dash-dotted lines), 192^3 (dash-dot-dotted lines), and the three-dimensional spectra $E(k)$ (solid lines), respectively.

In the present study, we apply the initial energy spectrum, which is proposed by the latest experiments of Kang *et al.*³¹ in order to get insights into homogeneous turbulence and to render comparison between LES-LBM results and the experimental measurement more relevant. The initial three-dimensional energy spectrum is a smooth fit function that is represented by

$$E(k) = \beta c_K \varepsilon_0^{2/3} k^{-5/3} [kl_0 / [(kl_0)^{\alpha_2} + \alpha_1]]^{1/\alpha_2} [5/3 + \alpha_3] \times \exp(-\alpha_4 k \eta_0) \times \left[1 + \alpha_5 \left(\frac{1}{\pi} \arctan\{\alpha_6 \log_{10}(k \eta_0) + \alpha_7\} + \frac{1}{2} \right) \right], \quad (24)$$

where c_K and α_i are arbitrary coefficients fixed using with experimental data, yielding $c_K = 1.613$, $\alpha_1 = 0.39$, $\alpha_2 = 1.2$, $\alpha_3 = 4.0$, $\alpha_4 = 2.1$, $\alpha_5 = 0.522$, $\alpha_6 = 10.0$, and $\alpha_7 = 12.58$. The parameters l_0 , η_0 , and ε_0 (the integral scale, the Kolmogorov scale, and the dissipation, respectively) depend on the position of the probe in the experiments.³¹ β is a parameter introduced to rescale the intensity of the turbulence. We choose their nondimensional values at the position $x_1/M = 20$ in Kang's data, using the root-mean-square (rms) velocity and $M/2\pi$ as the velocity scale and the length scale, respectively. Then we have $l_0 = 10.416$, $\eta_0 = 4.58 \times 10^{-3}$, and $\varepsilon_0 = 0.103$.

The amplitude of the modes of initial velocity components in wave-number space are obtained from the above energy spectrum. The phase of the spectral components is initialized by random numbers. The minimum and maximum wave numbers resolved in the present simulations are $k_{\min} = 1$ and $k_{\max} = N/2$. Here, we test some different resolution cases. The initial energy spectrum from Eq. (24) and those one- and three-dimensional energy distributions from the inverse calculation from initial velocity field are given at Fig. 1. The initial condition for the present simulations is physical and hence results after short time are relevant.

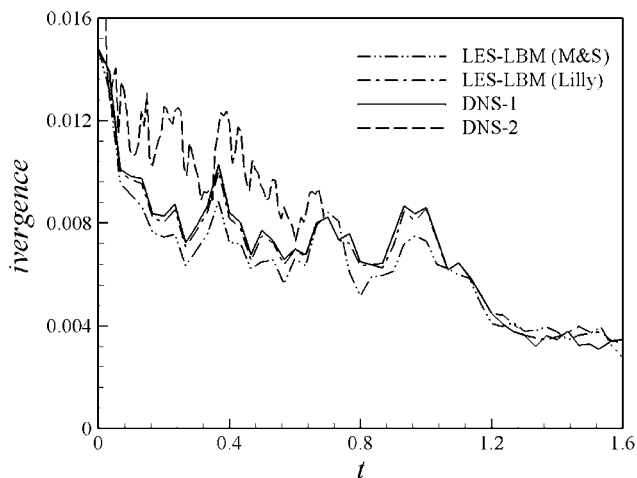


FIG. 2. Evolution of the maximum divergence with time. Here and in the following figures, (Lilly) denotes the traditional Smagorinsky model suggested by Lilly (Ref. 36) and (M&S) denotes the IR consistent model by Meyers and Sagaut (Ref. 29).

It is crucial to implement initialization of the velocity field in the DNS-LBM and LES-LBM of DHIT in a numerically consistent way. The Fourier transform FFT procedure is applied to the energy spectrum (24) to obtain the initial velocity field in physical space, which is used to initialize the distribution function for the LBM simulations. Although the velocity is divergence-free in Fourier space, it is not always strictly solenoidal in discrete physical space. The result is that the pressure and the velocity fluctuations grow quickly from the beginning of the calculation and lead to collapse of the entire solution. The strategy used here to obtain a numerically consistent initial velocity field is to solve a Poisson equation to project the non-solenoidal velocity field onto a solenoidal one. All present simulations are observed to lead to a physical development of low-Mach number turbulence (recall that LBM mimics compressible Navier–Stokes equations) when the procedure is implemented as shown in Fig. 2. Another procedure for the same purpose is proposed by Mei *et al.*³⁸ A detailed discussion regarding the initial conditions and boundary conditions in lattice Boltzmann simulations is available in the study of Skordos.³⁹

IV. RESULTS AND DISCUSSION

We perform LES-LBM of decaying homogeneous isotropic turbulence with both the classical Lilly–Smagorinsky model (results being denoted with “Lilly” in some figures) and the inertial-range (IR) consistent Smagorinsky model

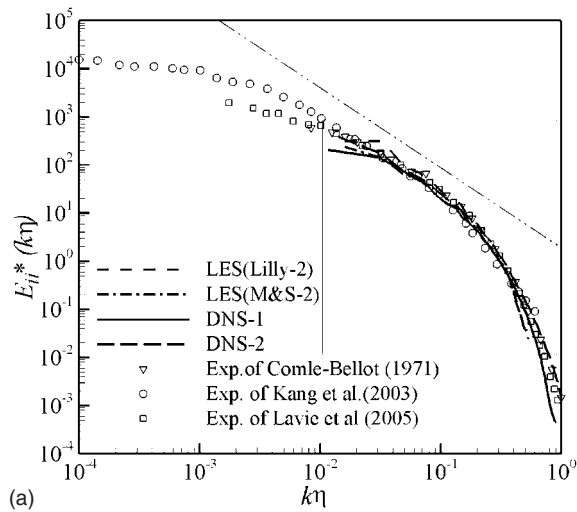
(denoted by “M&S” in figures). We also perform DNS-LBM of DHIT with two resolutions to enable accurate comparisons. Table I summarizes some basic parameters of our simulations including the mesh resolutions, the initial Taylor-scale Reynolds number, the kinetic viscosity coefficients, β , and the Smagorinsky constant C for LES cases. By considering the Taylor hypothesis, several experiments^{31,40,41} of spatially developing grid turbulence are made analogous to the current temporally decaying turbulence. In this section, we investigate detailed numerical statistical quantities and instantaneous data and test the performance of both eddy-viscosity SGS models in the framework of LBM. The influence of model coefficients and grid resolutions is also investigated. In addition, both versions addressing the computing strain rate \bar{S} in Sec. II B have been tested in our LES cases. We find that the difference in statistical quantities is negligible while the computational costs of the two methods are very similar (not shown here). Therefore, it was chosen to compute strain rate \bar{S} directly from the second moment of nonequilibrium distribution functions according to Eqs. (14) and (16) in cases Lilly-1 and Lilly-2, and to compute strain rate \bar{S} using FDM for all M&S cases.

A. Instantaneous energy spectra

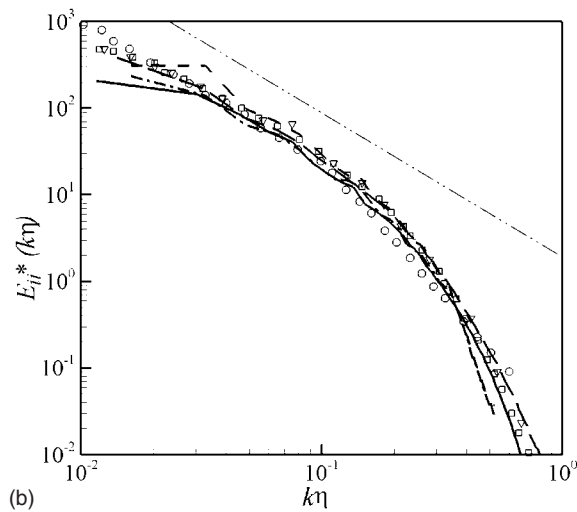
Here we show results from a set of simulations in which the initial spectrum is given by Eq. (24). The present simulations start from the initial conditions outlined above in Sec. III. First of all, the energy spectra from DNS-LBM and LES-LBM with both models (Lilly or M&S) are presented. Figure 3 compares the longitudinal one-dimensional energy spectra $E_{11}^*(k\eta)$ of Comte-Bellot and Corrsin⁴⁰ and of Lavoie *et al.*⁴¹ as well as of Kang *et al.*³¹ (Refs. 40 and 41 deal with moderate and low Re_λ , $Re_\lambda \leq 150$, and $Re_\lambda \leq 55$, respectively, and the experiments of Ref. 31 were performed at high Re_λ , $Re_\lambda \approx 600$ –700). Here, the universal nondimensional Kolmogorov spectrum function $E_{ii}^*(k\eta) = E_{ii}(k\eta) / (\eta v_\eta^2)$ is computed using the theoretical energy spectra of Pope,³⁷ and v_η is the Kolmogorov velocity. The Kolmogorov scale is used to normalize the wavenumber axis in order to make relevant comparisons between the different reference data sets. Since inertial-range consistency is directly linked to the capability of the subgrid models to capture finite Reynolds number effects, it is relevant to put the emphasis on the high wavenumber part of the spectrum and to check the capability of the IR Smagorinsky model to predict a physical shape of the kinetic energy spectrum in cases in which the LES filter cutoff is not located within the Kolmogorov inertial range. The calculated

TABLE I. Basic simulation parameters as discussed in Sec. IV.

CASES	DNS-1	DNS-2	Lilly-1	Lilly-2	M&S-1	M&S-2	M&S-3
N	128	192	64	64	64	64	96
ν_0	3.3×10^{-4}	3.1×10^{-4}	4×10^{-4}	4×10^{-4}	4×10^{-4}	4×10^{-4}	3.5×10^{-4}
Re_λ	101	96	96	103	89	102	101
β	0.07	0.07	0.07	0.07	0.07	0.07	0.07
C			0.10	0.18	0.10	0.18	0.18



(a)



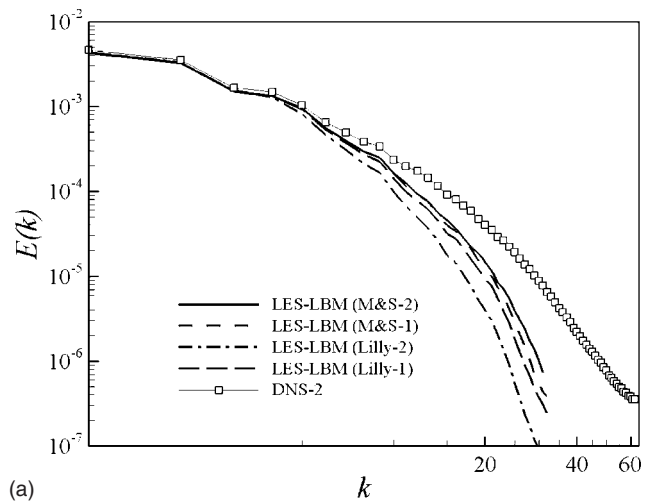
(b)

FIG. 3. One-dimensional energy spectra $E_{ii}^*(k\eta) = E_{ii}(k\eta) / (\eta v_k^2)$ normalized in Kolmogorov units. (b) is the enlarged part from (a). Dash-dot-dotted line: Slope of $-5/3$.

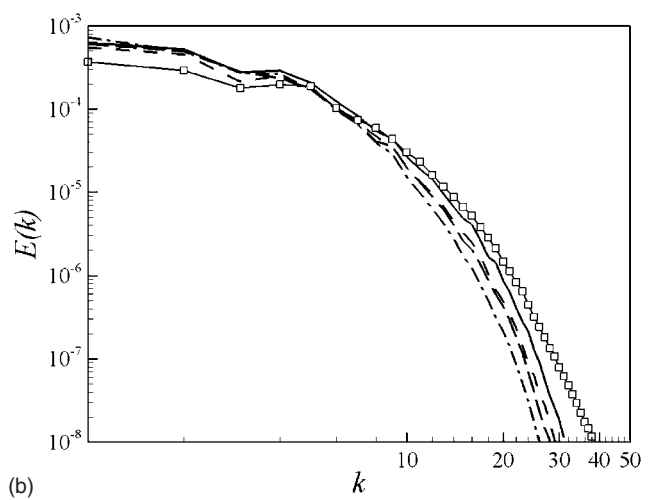
normalized spectra are in good agreement with those obtained in the experiments in the range of $2 \times 10^{-2} \leq k\eta \leq 6 \times 10^{-1}$.

Figure 4 displays the three-dimensional instantaneous energy spectra with different LES-LBM cases and DNS-LBM cases for 192.³ The LES spectra are compared against DNS spectrum at the same time. The IR consistent model with $C=0.18$ performs better than the other models in the different time. It also yields a better prediction of time evolution of the statistical quantities (see the discussion in Sec. IV B). We find that the spectrum of using the Lilly model with $C=0.18$ leads to larger discrepancies either in Fig. 4(a) or in Fig. 4(b). For this reason, we put off presenting other results from this case ($C=0.18$, Lilly-2) until further discussion in the next section.

Next, we examine the behavior of the energy spectrum obtained by LES-LBM with the IR consistent model. The decay of the one-dimensional energy spectra is shown in Fig. 5(a). The plots reported are in the same time interval as $\delta t = 0.05$. The spectra present similar features with each other but the inertial region is hard to observe in the calculated



(a)



(b)

FIG. 4. The instantaneous three-dimensional energy spectra at (a) $t=0.05$ and (b) $t=0.18$ obtained from DNS-LBM (192³) and LES-LBM with different SGS models (Lilly and M&S).

spectra, as expected for the Reynolds number range. Figure 5(b) shows the normalized one-dimensional energy spectra in Kolmogorov units, which correspond to the spectra of Fig. 5(a). The collapse of the various time spectra in the Kolmogorov units is excellent in the viscous range where $k\eta > 0.1$. Similar agreement was also reported by Comte-Bellot and Corrsin⁴⁰ and our DNS-LBM results as well as Djenidi's DNS²¹ of grid-generated turbulence. It indicates that the self-similar decaying regime exists in energy spectra when Re_λ changes with t , and corroborates the self-preserving state in decaying isotropic turbulence discussed by Burattini *et al.*²²

B. Time evolution of various statistics

The corresponding effective relaxation factors for all the cases in Table I following Eqs. (16) and (22) are as shown in Fig. 6 as a function of time steps. All of them relax toward the constant value of DNS at the final stage of decay. The LES-LBM is based on an instantaneous adjustment of the relaxation time, which is the key difference between the Smagorinsky model implemented in LES-LBM and Navier-Stokes LES. In LES-LBM, the subgrid stress relaxes to the

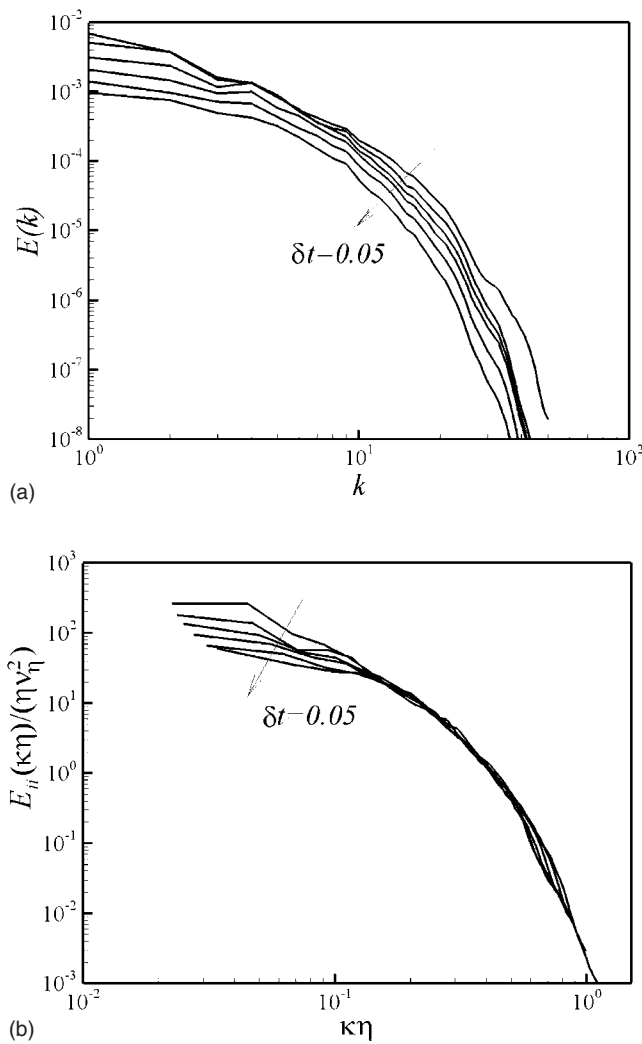


FIG. 5. Time evolution of instantaneous three-dimensional energy spectra at equal intervals (a), and the normalized one-dimensional energy spectra in Kolmogorov units (b), starting from $t=0.0025$ and the interval of time is $dt=0.05$, with the IR consistent Smagorinsky model.

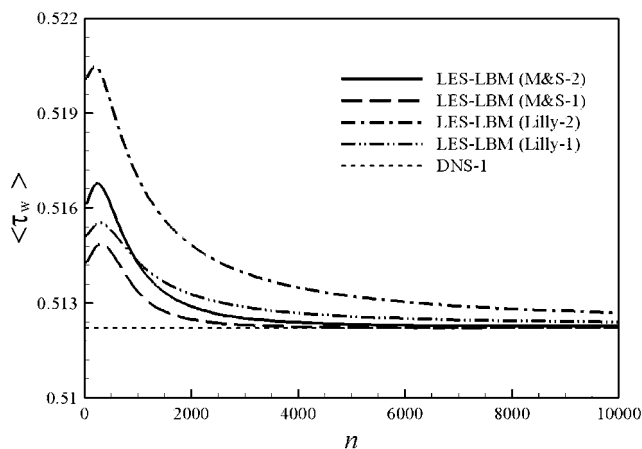


FIG. 6. Evolution of the spatial-average effective relaxation time of the LBM vs time steps.

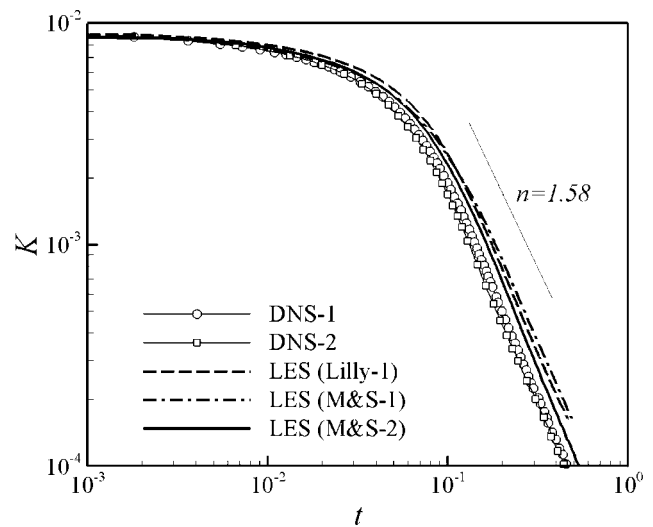


FIG. 7. The total turbulent kinetic energy at different resolutions using LES-LBM and DNS-LBM.

value imposed by resolved strain with a relaxation time determined by the current eddy-viscosity. In this sense, the stress is not in instantaneous equilibrium with resolved strain. Thus, we agree with the statement by Yu *et al.*²³ that the LES-LBM may have inherent space-time memory features. It should be noticed that $\langle \tau_w \rangle$ here is spatial average value of $\tau_w(x, t)$.

Figures 7 and 8 show the time evolution of total turbulent kinetic energy K and the dissipation rate ε given by three LES-LBM cases and both DNS-LBM for 128^3 and 192^3 , respectively. K is defined and calculated as

$$K = \int_0^{\pi/\Delta_L} E(k) dk = \langle u'^2 + v'^2 + w'^2 \rangle / 2. \quad (25)$$

The decay exponent of $K(t)$ in numerical experiment can be seen in the moving frame according to the Taylor approximation,

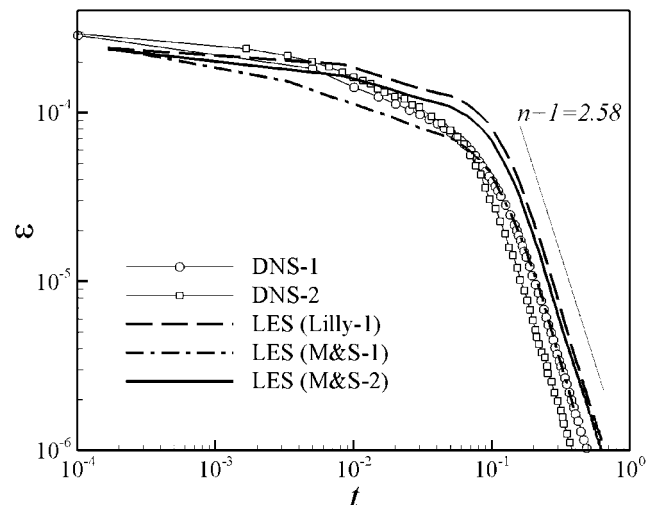


FIG. 8. The dissipation rate at different resolutions using LES-LBM and DNS-LBM.

$$K(t) = K_0(t_0) \left(\frac{t}{t_0} \right)^{-n}. \quad (26)$$

In this expression, K_0 is the turbulent kinetic energy at an arbitrary time t_0 and n is a universal exponent.

It is well known that the energy decay exponent is closely related to the low wavenumber portion of the three-dimensional spectrum, and is affected by many features of the initial spectrum as well as Re_λ .¹² Saffman¹³ suggested that for DHIT in which the low wavenumber portion of the spectrum goes as k^2 , the low Reynolds number exponent was shown to be $3/2$ and the high Reynolds number exponent limit to be $6/5$, which is commonly observed in experiments. For example, Kang *et al.*³¹ reported $n=1.25$ for their decaying grid-generated turbulence at high Reynolds number (the initial Re_λ approaches 700). Batchelor and Townsend¹² presented the first analysis and experiments for very low Reynolds number decaying turbulence and suggested that the exponent should be $5/2$ in the final period of decay.

The decay exponent law from present LES simulations is $n \approx 1.58$, which is in agreement with both DNS results and is close to the value of Djenidi's DNS²¹ ($n \approx 1.53$). The large-eddy simulation study of DHIT by Sagaut and Ciardi²⁰ gave $n \approx 1.59$ for variational multiscale models and they obtained results $n \approx 1.61$ for the dynamic Smagorinsky model. Our results are also close to Lavoie's measurements,⁴¹ which show that the total kinetic energy is proportional to $t^{-1.5}$. On the other hand, comparison of the DNS results between resolution 128^3 and that obtained using a finer mesh 192^3 does not reveal obvious differences in the statistical turbulent kinetic energy considered in this paper.

The dissipation rate in Fig. 8 is evaluated numerically here in wavenumber space as

$$\varepsilon(t) = 2\nu \int_0^{\pi/\Delta_L} k^2 E(k, t) dk. \quad (27)$$

And, according to the power law of $K(t)$ [Eq. (26)], the dissipation rate can be written in physical space as

$$\varepsilon(t) = -\frac{dK(t)}{dt} = -\left(\frac{nK_0(t_0)}{t_0} \right) \left(\frac{t}{t_0} \right)^{-(n+1)}. \quad (28)$$

According to the previous theoretical analysis, the Smagorinsky model underpredicts the dissipation rate more or less. Figure 8 shows that the collapse of ε predicted by both Smagorinsky models is really slower than the DNS value. The phenomenon corresponds to the evolution of the energy spectrum in Fig. 4. The IR consistent models yield results closer to the DNS ones. The decay exponent $n+1$ is estimated to be 2.58 in our simulations, so we know that the decaying exponent law of the enstrophy H is 2.58 from $\varepsilon = 2\nu H$ in homogeneous turbulence. From both figures, we find that the IR Smagorinsky model (solid line, $C=0.18$) yields the best results among all LES cases, and the Lilly–Smagorinsky model (long dot-dashed line, $C_S=0.10$) presents better results than other LES cases except the M&S-2 case. It should be noted that in the absence of a production

term, the kinetic energy E_k and the dissipation rate ε both decay monotonically in time (this is also observed with the measurements of Kang *et al.*³¹ and the DNS data of Djenidi²¹ in grid turbulence). There is an obvious difference in the behavior of ε between the present result and another study by Yu *et al.*²³ The dissipation rate ε decays monotonically with time here, whereas it increases in an early stage under another initial condition in Yu *et al.*'s study. This source of the discrepancy comes from the different initial energy spectrum. The analysis of Saffman¹³ explained that the details of the cascade and dissipation rate are influenced by the shape of the energy spectrum.

Once we obtained kinetic energy K and the dissipation rate ε from Eqs. (25) and (27), the Taylor scale and the Kolmogorov scale are given by

$$\lambda = \frac{\sqrt{10K}^{1/2}}{(\varepsilon\nu)^{1/4}} \eta, \quad (29)$$

$$\eta = (\nu^3/\varepsilon)^{1/4}. \quad (30)$$

The Taylor length scale λ is the characteristic length scale for the entire spectrum. The Reynolds number based on the Taylor scale is

$$Re_\lambda = \sqrt{\frac{2}{3}} \frac{K^{1/2} \lambda}{\nu}. \quad (31)$$

The evolution of Taylor and Kolmogorov microscales (λ and η , respectively) and the Taylor-scale Reynolds number are calculated and shown in Figs. 9(a)–9(c). As expected, with the energy of isotropic turbulence decaying, λ and η grow with time as shown in Figs. 9(a) and 9(b), and the resulting Reynolds number Re_λ decreases with decay [Fig. 9(c)]. In Figs. 9(a) and 9(c), there is a high value of λ and Re_λ after the initial time even η increases monotonously at entire decay. The phenomenon reflects the inverse transfer of energy between the small scales and larger structures and which is also confirmed by the simulation of grid-generated turbulence.³¹ It should be pointed out that all these quantities increase or decrease monotonously if an isotropic Gaussian field is prescribed at initial time rather than the nearly fully developed initial field taken from experiment. This phenomenon implies that the effect of initial field on the evolution of small scale in the decay may not be neglected. The computed ratio λ/η decreases slowly from 17 to 10 with energy decay. This trend shows consistency in the asymptotic relation $(\lambda/\eta)_{iso} = (30 Re_\lambda)^{1/4}$ and the experimental values by Lavoie *et al.*,⁴¹ which decrease from $x_1/M=20$ to $x_1/M=60$.

It is noted that the Taylor microscale given by DNS behaves close to the square root of time, i.e., $\lambda \propto t^{1/2}$ for the final period of decay, as shown in Fig. 10. The result is consistent with the asymptotic behavior of George's theoretical prediction⁴² of DHIT. They argue that λ should follow the $1/2$ -law of the decaying time if a correct power law of kinetic energy exists. However, we cannot affirm that this microscale given by LES is consistent with the theoretical prediction.⁴² In the present LES cases, the lowest Reynolds

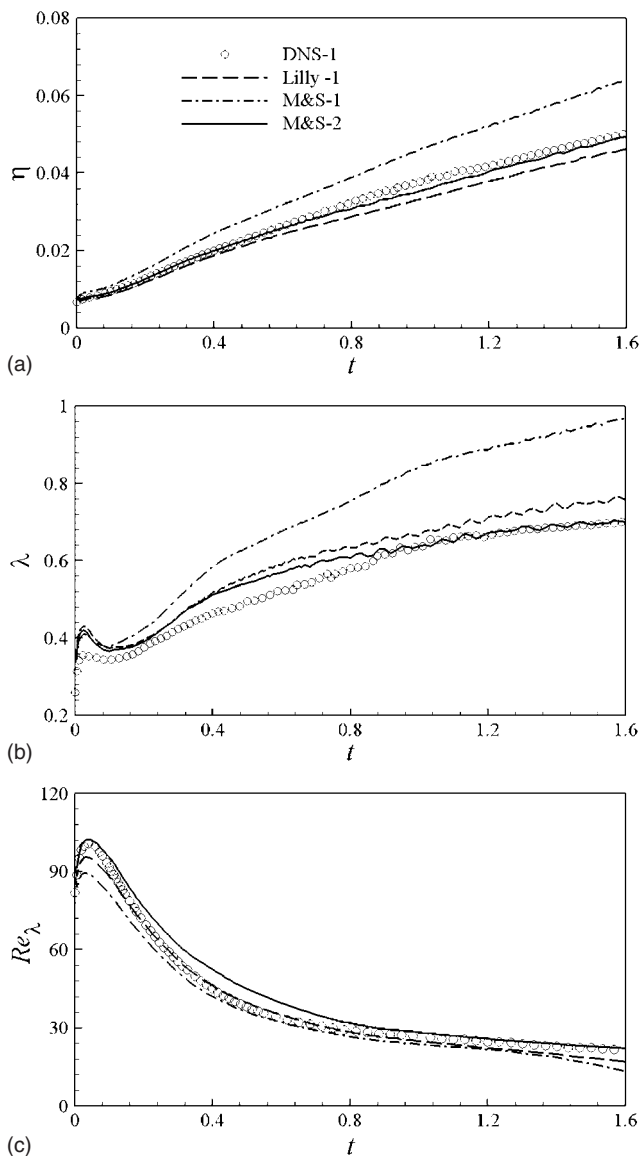


FIG. 9. The variations of Taylor length scale (a), Kolmogorov microscales (b), and Taylor-scale Reynolds numbers (c) of the decaying isotropic turbulence.

number during the final decaying stage is about 6, but the LES may give an unphysical solution when the Reynolds number is very small since the integral scales grow and eventually become comparable to the domain length, result in pseudo kinetic energy pileup. This is why they have some difficulties to reproduce 1/2-law at the final period of decay.

To discuss further the behavior of the model coefficients for the Lilly–Smagorinsky model and the IR consistent model, the time variation of the ratio Δ/η is presented in Fig. 11. We also give the variations of the Smagorinsky coefficient C as a function of the ratio Δ/η .²⁹ The ratio ranges for DNS are $(\Delta/\eta)_{\min}=0.98$ to $(\Delta/\eta)_{\max}=6.54$ and for LES they are $(\Delta/\eta)_{\min}=1.96$ to $(\Delta/\eta)_{\max}=13.08$ during the dominating decaying period for our cases. The ratio could correspond to the good quality of C^* as an approximation to C in the IR model. For $(\Delta/\eta)_{\max} \approx 13$ at the beginning of the decay, the coefficient advocated is $C_1=0.15$ and $C_2 \approx 0.10$ for

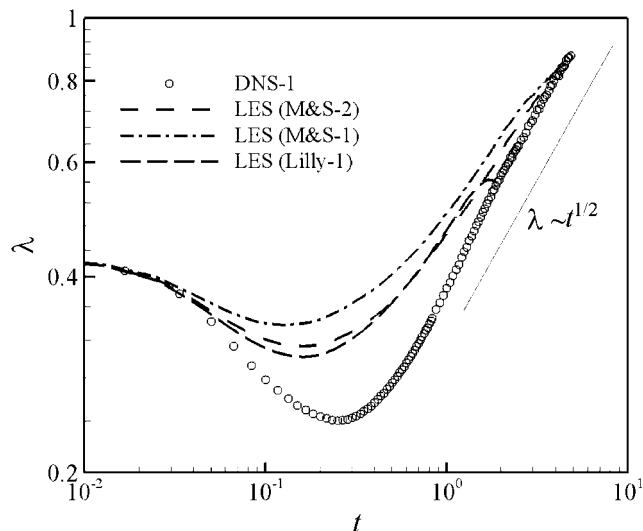


FIG. 10. The Taylor microscales vs time in logarithm-logarithm scales at the final period of decay of turbulence.

$(\Delta/\eta)_{\min} \approx 6$. This in turn may explain why the results of the IR consistent model with $C=0.10 \sim 0.18$ are closer to those of DNS than the classical Lilly model (see Figs. 7–9). This would corroborate the previous discussion on how the behavior of the model coefficients depends on the ratio of the filter width and the Kolmogorov scale.

C. The velocity derivative skewness and flatness

As typical high-order structure functions, the flatness of the velocity derivatives du_i/dx_i ,

$$F_{ii} = \frac{\langle (\partial u_i / \partial x_i)^4 \rangle}{\langle (\partial u_i / \partial x_i)^2 \rangle^2}, \tag{32}$$

and the skewness of the velocity derivatives du_i/dx_i ,

$$S_{ii} = - \frac{\langle (\partial u_i / \partial x_i)^3 \rangle}{\langle (\partial u_i / \partial x_i)^2 \rangle^{3/2}}, \tag{33}$$

are important characteristics of isotropic turbulent flow. The latter is directly related to the production of dissipation and the energy transfer term through the relationship³⁷

$$\left\langle \left(\frac{\partial u_i}{\partial x_i} \right)^3 \right\rangle = - \frac{2}{35} \int_0^\infty k^2 T(k) dk. \tag{34}$$

The evolution of the velocity derivative skewness and flatness starting from the initial condition are evaluated with LES-LBM and DNS-LBM here as shown in Figs. 12(a) and 12(b), respectively. The magnitude of the flatness tensor quickly comes to a level between 3.5 and 4.0 for our DNS and LES results at the forepart period of decay as shown in Fig. 12(b). Skewness is always negative due to the energy cascade of resolved scales except it is statistically zero at the initial field. Kolmogorov’s theory³⁴ for decay of isotropic turbulence yielded the results that S in high Reynolds number turbulent flows should be constant. George⁴² argued that

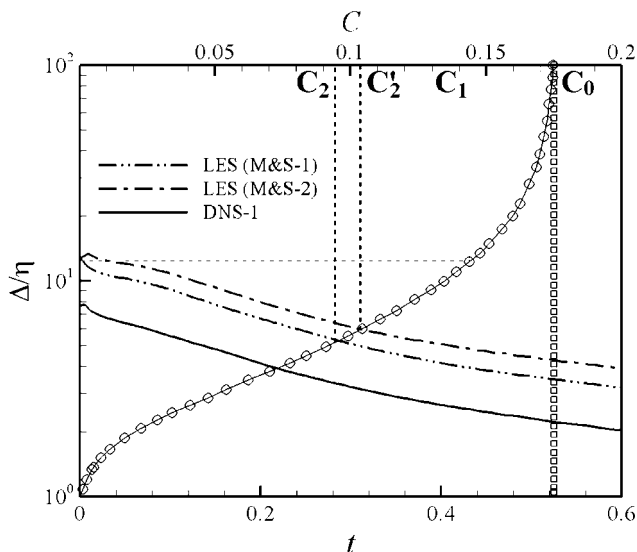


FIG. 11. The evolution of Δ/η with time and the evolution of C as a function of the ratio Δ/η . Circles: Coefficient C of the IR model by theoretical analysis from Eq. (16) or Eq. (2.18) of Ref. 29. Squares: Lilly's Smagorinsky constant $C_0=0.18$, C_1 , and $C_2(C_2')$ corresponds to $t=0.0$ and $t \approx 0.3$, respectively, for the IR model.

the skewness should vary with Reynolds number and time during decay as Re_λ^{-1} or $t^{-(n'+1)/2}$. Our DNS-LBM result gives a value of the skewness close to -0.5 [Fig. 12(a)], which is consistent with some experiments⁴² and DNS (Refs.

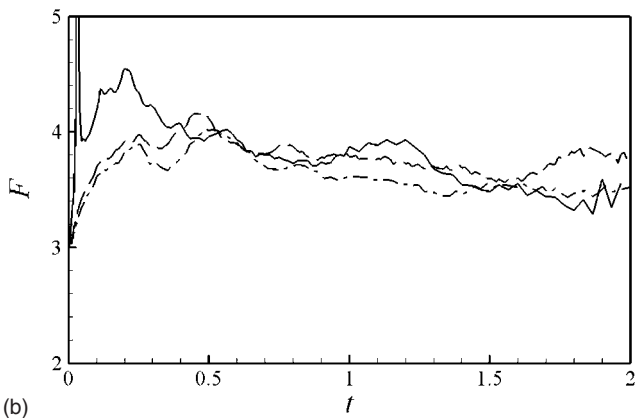
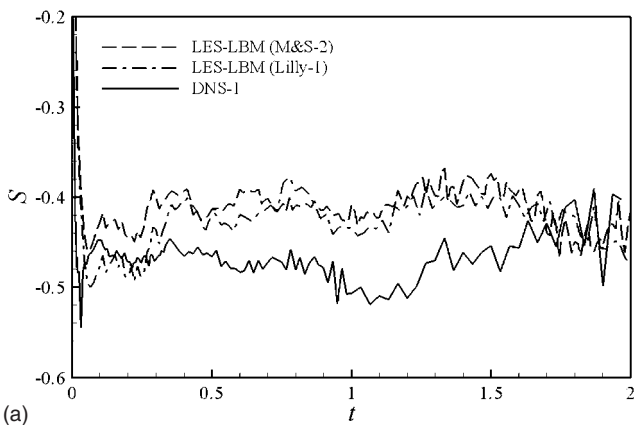


FIG. 12. The velocity derivative skewness (a) and flatness (b). The value shown here is quantified by $F=(F_{11}+F_{22}+F_{33})/3$ and $S=(S_{11}+S_{22}+S_{33})/3$.

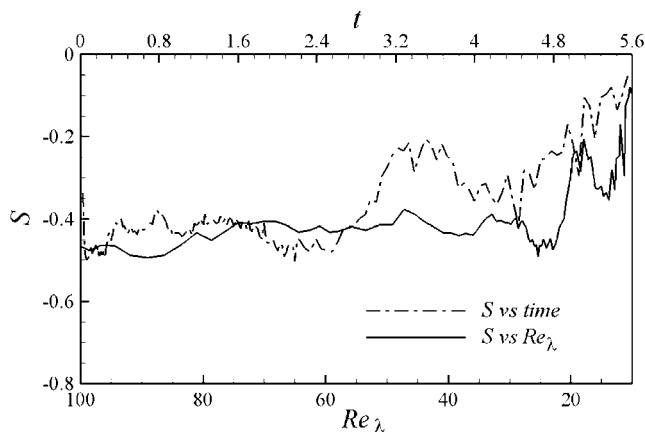


FIG. 13. The velocity-derivative skewness as a function of both Re_λ (solid line) and time (dashed line) by LES-LBM (M&S-2).

21 and 43) in a certain range of the Reynolds number. However, both LES-LBM cases give a value approximately equal to -0.4 at the forefront period of decay [Fig. 12(a)]. We notice that Kang *et al.*³¹ reported that the skewness of longitudinal velocity increments measured at $x_1/M=40$ is between -0.38 and -0.24 . The behavior of skewness at low Reynolds numbers is of interest since it implies the rate at which the non-linear energy transfer vanishes as Re_λ decreases.

Figure 13 displays the skewness as a function of both Re_λ and computational time t for LES with the IR consistent model. The skewness S exhibits a plateau approximately when $Re_\lambda \geq 20$, which implies that the flow field behaves like developed isotropic turbulence at this stage,³⁴ and then it tends to zero at the final period of decay ($Re_\lambda \rightarrow 0$, theoretically, but $Re_{\lambda min} > 6$ in the present LES due to its limitation), which is agreement with those measured by Tavoularis, Bennett, and Corrsin.⁴⁴ Interestingly, the behavior of velocity derivative skewness varies with t and Re_λ when all of them are drawn in a log-log scale as in Figs. 14(a) and 14(b). The current result seems to be in agreement roughly with the consequences of George's self-preservation theory⁴² as $S \sim t^{-(n'+1)/2}$ and $S \sim Re_\lambda^{-1}$ in current ranges of t and Re_λ .

D. Effect of grid resolutions

The effect of mesh resolution on the LES-LBM is studied by comparing two LES cases with the IR consistent model on different mesh points in 64^3 and 96^3 ; the initial value of the Reynolds number is about 108. Figure 15 shows the evolution of total kinetic energy E_k and the dissipation rate ϵ . Clearly, the E_k and ϵ given by 96^3 are consistently closer to the DNS than that by 64^3 . Comparisons of the power law of E_k and ϵ , both cases of 96^3 and 64^3 , all give satisfactory values during the period of decay. However, the coarser resolution of 64^3 overestimates the value at the final period of decay, which is remarkable relatively in the estimation of the dissipation rate. The slight deviation also corresponds to the behavior of the instantaneous energy spectrum versus low wavenumber in the different decay stage (t_1 and t_2) as shown in Fig. 16.

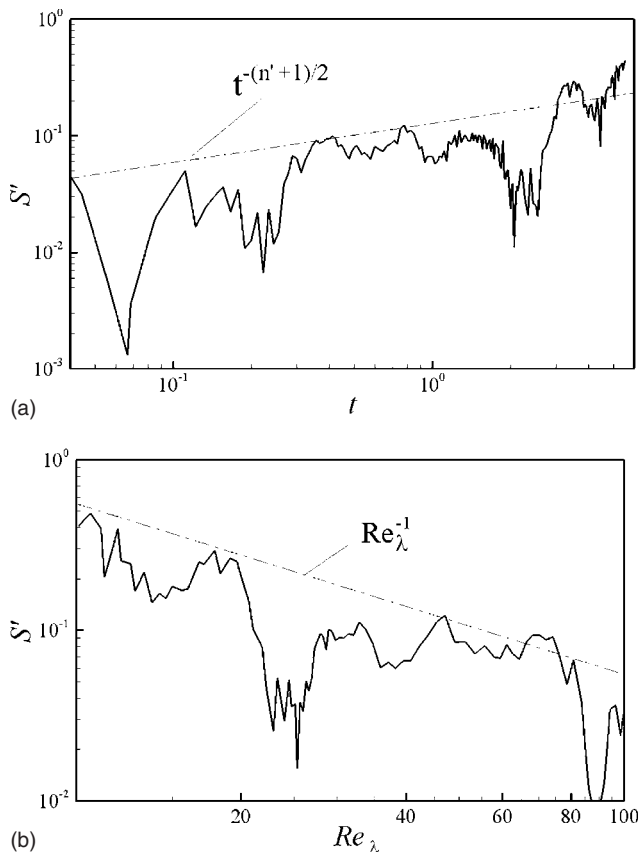


FIG. 14. The velocity-derivative skewness ($S'=S+0.5$, $n'=-1.58$) vs time in log-log scale (a), S' vs Re_λ in log-log scale, and (b) by LES-LBM with the M&S-2 model ($C_s=0.18$).

V. CONCLUDING REMARKS

In the present paper, we extended the study of the decaying homogeneous isotropic turbulence with large-eddy simulation based on the lattice Boltzmann equation, and we investigated the performance of the standard Lilly–Smagorinsky model and the IR consistent Smagorinsky model. The results are assessed via comparisons with the theory and the experimental data as well as DNS data. A very encouraging result is that the well known decay exponents of the kinetic energy and the dissipation rate are reproduced. Other results are found to be consistent with simulations made by different numerical schemes and measurements of grid turbulence.

We investigated further the behavior of the models and the effect of the model coefficients by analysis for statistical quantities of decaying isotropic turbulence from a numerical and a physical point of view. The Smagorinsky coefficients depend on the local ratio of the filter width Δ to the Kolmogorov scale η , according to what the analysis of Meyers and Sagaut²⁹ suggests. By evaluating the model coefficients as functions of the subgrid activity, the present results of the LES-LBM bases on the IR consistent model exhibit more satisfactory behavior than a classical one when compared with DNS and other methods. We also examine in particular the developments of the energy spectra and the velocity-derivative skewness as a function of Reynolds number and decaying time. The present results demonstrate that the IR

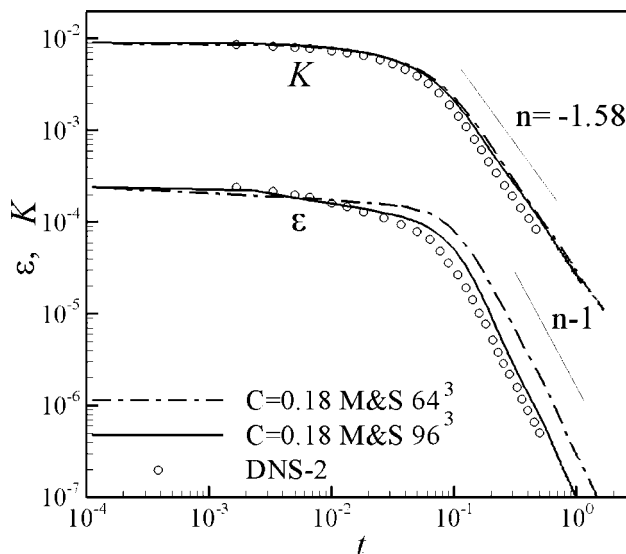


FIG. 15. Time evolution of the total kinetic energy and the dissipation rate with different grid resolutions ($N=64$ and 96) using LES-LBM (IR consistent Smagorinsky model $C_s=0.18$).

consistent model also provides an effective improvement. However, the effects of time-space correlations should be investigated further, and the effects of the initial conditions may still be of concern.

It is crucial to maintain a consistent and nearly solenoidal initial velocity field. In addition, it was shown that there is only a slight discrepancy between the two different methods (described in Secs. II B and II C) to evaluate the strain rate tensor, and the computing time of both methods is almost identical.

Overall, the present study provides detailed numerical data and analysis against which such various subgrid-viscosity SGS models can be tested in the frame of the LBM. We recall that LES-LBM is a potentially viable tool for the study of turbulent flows and should be given more attention to develop reasonable turbulence models.

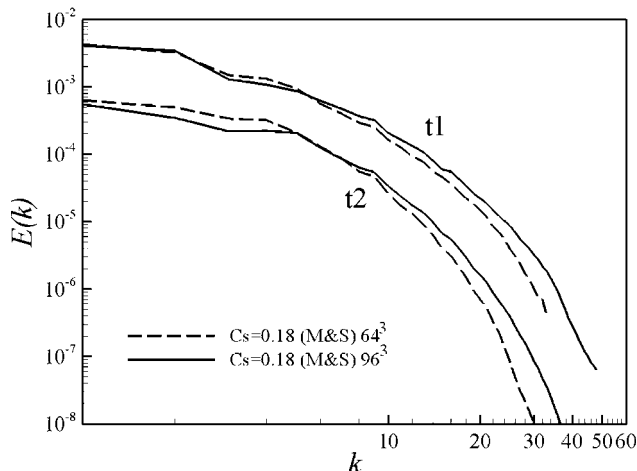


FIG. 16. Evolution of instantaneous three-dimensional energy spectra with different grid resolutions (the cubic of 64 and 96) at $t1=0.05$ and $t2=0.20$ using LES-LBM (M&S Smagorinsky model $C_s=0.18$).

ACKNOWLEDGMENTS

Many helpful discussions with Dr. D. Ricot (Technocentre Renault), Dr. A. Toutant, and M. Krawczyk are warmly acknowledged. This work was supported by ADEME within the PREDIT MIMOSA Project. The first author (Y.-H.D.) also acknowledges the support of the Natural Science Foundation of China (Grant No. 10772109).

- ¹S. Chen and G. D. Doolen, "Lattice Boltzmann method for fluid flows," *Annu. Rev. Fluid Mech.* **30**, 329 (1998).
- ²D. Yu, R. Mei, L. Luo, and W. Shyy, "Viscous flow computations with the method of lattice Boltzmann equation," *Prog. Aerosp. Sci.* **39**, 329 (2003).
- ³G. R. McNamara and G. Zanetti, "Use of the Boltzmann equation to simulate lattice-gas automata," *Phys. Rev. Lett.* **61**, 2332 (1988).
- ⁴Y. Qian, D. d'Humieres, and P. Lallemand, "Lattice BGK models for Navier–Stokes equations," *Europhys. Lett.* **17**, 479 (1992).
- ⁵R. Benzi, S. Succi, and M. Vergassola, "The lattice Boltzmann equation: Theory and applications," *Phys. Rep.* **222**, 145 (1992).
- ⁶H. Chen, S. Chen, and H. W. Matthaeus, "Recovery of the Navier–Stokes equation using a lattice Boltzmann method," *Phys. Rev. A* **45**, R5339 (1992).
- ⁷R. Benzi and S. Succi, "Two-dimensional turbulence with the lattice Boltzmann equation," *J. Phys. A* **23**, L1 (1990).
- ⁸R. Benzi, M. V. Struglia, and R. Tripiccion, "Extended self-similarity in numerical simulations of three-dimensional anisotropic turbulence," *Phys. Rev. E* **53**, R5565 (1996).
- ⁹J. M. G. Eggels, "Direct and large-eddy simulation of turbulent fluid flow using the lattice Boltzmann scheme," *Int. J. Heat Fluid Flow* **17**, 307 (1996).
- ¹⁰S. Hou, J. Sterling, S. Chen, and G. D. Doolen, "A lattice Boltzmann subgrid model for high Reynolds number flows," in *Pattern Formation and Lattice Gas Automata*, edited by A. T. Lawniczak and R. Kapral, Fields Institute Communications Vol. 6 (AMS, Providence, 1996), pp. 151–166.
- ¹¹M. Krawczyk, J. Tölke, and L. S. Luo, "Large-eddy simulations with a multiple-relaxation time LBE model," *Int. J. Mod. Phys. B* **17**, 33 (2003).
- ¹²G. K. Batchelor and A. A. Townsend, "Decay of turbulence in the final period," *Proc. R. Soc. London, Ser. A* **194**, 527 (1948).
- ¹³P. G. Saffman, "The large scale structure of homogenous turbulence," *J. Fluid Mech.* **27**, 581 (1967).
- ¹⁴S. A. Orszag and G. S. Patterson, "Numerical simulation of three-dimensional homogeneous isotropic turbulence," *Phys. Rev. Lett.* **28**, 76 (1972).
- ¹⁵M. S. Mohamed and J. C. LaRue, "The decay power law in grid-generated turbulence," *J. Fluid Mech.* **219**, 195 (1990).
- ¹⁶N. N. Mansour and A. A. Wray, "Decay of isotropic turbulence at low Reynolds number," *Phys. Fluids* **6**, 808 (1994).
- ¹⁷C. Seror, P. Sagaut, C. Bailly, and D. Juvé, "Subgrid-scale contribution to noise production in decaying turbulence," *AIAA J.* **38**, 1795 (2000).
- ¹⁸M. Oberlack, "On the decay exponent of isotropic turbulence," *Proc. Appl. Math. Mech.* **1**, 294 (2002).
- ¹⁹P. Sagaut and V. Levasseur, "Sensitivity of spectral variational multiscale methods for large-eddy simulation of isotropic turbulence," *Phys. Fluids* **17**, 035113 (2005).
- ²⁰P. Sagaut and M. Ciardi, "A finite-volume variational multiscale method coupled with a discrete interpolation filter for LES of isotropic turbulence and fully developed channel flow," *Phys. Fluids* **18**, 115101 (2006).
- ²¹L. Djenidi, "Lattice Boltzmann simulation of grid-generated turbulence," *J. Fluid Mech.* **552**, 13 (2006).
- ²²P. Burattini, P. Lavoie, A. Agrawal, L. Djenidi, and R. A. Antonia, "Power law of decaying homogeneous isotropic turbulence at low Reynolds number," *Phys. Rev. E* **73**, 066304 (2006).
- ²³H. Yu, S. S. Girimaji, and L. S. Luo, "DNS and LES of decaying isotropic turbulence with and without frame rotation using lattice Boltzmann methods," *J. Comput. Phys.* **209**, 599 (2005).
- ²⁴K. Lee, D. Z. Yu, and S. S. Girimaji, "Lattice Boltzmann DNS of decaying compressible isotropic turbulence with temperature fluctuations," *Int. J. Comput. Fluid Dyn.* **20**, 401 (2006).
- ²⁵D. Z. Yu and S. S. Girimaji, "Direct numerical simulations of homogeneous turbulence subject to periodic shear," *J. Fluid Mech.* **566**, 117 (2006).
- ²⁶S. S. Girimaji, "Boltzmann kinetic equation for filtered fluid turbulence," *Phys. Rev. Lett.* **99**, 034501 (2007).
- ²⁷M. Germano, U. Piomelli, P. Moin, and W. H. Cabot, "A dynamic subgrid-scale model," *Phys. Fluids A* **3**, 1760 (1991).
- ²⁸P. Sagaut, *Large Eddy Simulation for Incompressible Flows: An Introduction*, 3rd ed. (Springer, Berlin, 2005).
- ²⁹J. Meyers and P. Sagaut, "On the model coefficients for the standard and the variational multi-scale Smogorisky model," *J. Fluid Mech.* **569**, 287 (2006).
- ³⁰J. Meyers, P. Sagaut, and B. Geurts, "Optimal model parameters for multi-objective large-eddy simulations," *Phys. Fluids* **18**, 095103 (2006).
- ³¹H. S. Kang, S. Chester, and C. Meneveau, "Decaying turbulence in an active-grid-generated flow and comparisons with large-eddy simulation," *J. Fluid Mech.* **480**, 129 (2003).
- ³²P. L. Bhatnagar, E. P. Gross, and M. Krook, "A model for collision processes in gases. I. Small amplitude processes in charged and neutral one-component systems," *Phys. Rev.* **94**, 511 (1954).
- ³³S. Chen, Z. Wang, X. Shan, and G. D. Doolen, "Lattice Boltzmann computational fluid dynamics in three dimensions," *J. Stat. Phys.* **68**, 379 (1992).
- ³⁴A. N. Kolmogorov, "On degeneration (decay) of isotropic turbulence in an incompressible viscous liquid," *Dokl. Akad. Nauk SSSR* **31**, 538 (1941).
- ³⁵J. Smagorinsky, "General circulation experiments with the primitive equations. I: The basic experiment," *Mon. Weather Rev.* **91**, 99 (1963).
- ³⁶D. K. Lilly, "The representation of small-scale turbulence in numerical simulation experiments," in *Proceedings of the IBM Science Computing Symposium on Environmental Science*, edited by H. H. Goldstine (T. J. Watson Research Center, Yorktown Heights, 1967), pp. 195–210.
- ³⁷S. B. Pope, *Turbulent Flows* (Cambridge University Press, Cambridge, 2000).
- ³⁸R. Mei, L. S. Luo, P. Lallemand, and D. d'Humieres, "Consistent initial conditions for lattice Boltzmann simulations," *Comput. Fluids* **35**, 857 (2006).
- ³⁹P. A. Skordos, "Initial and boundary conditions for the lattice Boltzmann method," *Phys. Rev. E* **48**, 4823 (1993).
- ⁴⁰G. Comte-Bellot and S. Corrsin, "The use of a contraction to improve the isotropy grid-generated turbulence," *J. Fluid Mech.* **25**, 657 (1966).
- ⁴¹P. Lavoie, P. Burattini, L. Djenidi, and R. A. Antonia, "Effect of initial conditions on decaying grid turbulence at low Re_λ ," *Exp. Fluids* **39**, 865 (2005).
- ⁴²W. K. George, "The decay of homogeneous isotropic turbulence," *Phys. Fluids A* **4**, 1492 (1992).
- ⁴³N. N. Mansour and A. A. Wray, "Decay of isotropic turbulence at low Reynolds number," *Phys. Fluids* **6**, 808 (1994).
- ⁴⁴S. Tavoulari, J. C. Bennett, and S. Corrsin, "Velocity-derivative skewness in small Reynolds number, nearly isotropic turbulence," *J. Fluid Mech.* **88**, 63 (1978).